Metamaterial-enabled Fully On-Chip Polarization-Handling Devices

Yaotian Zhao, Jinlong Xiang, An He, Yu He, Xuhan Guo,* and Yikai Su

Polarization manipulation is essential in photonic integrated circuits and has numerous applications in various fields, such as optical communication, nonlinear optics, and quantum optics. Advances in nanofabrication have enabled the integration of subwavelength-structured metamaterials on optical waveguides, providing unprecedented optical manipulation capabilities beyond classical waveguide-based architectures. In this paper, the polarization space is demonstrated to be fully manipulated by a dielectric metamaterial composed of nanoholes and nanoslots. This approach offers competitive performances for key polarization components, including the polarizer, polarization beam splitter, and polarization-splitter-rotator, while maintaining ultra-compact coupling regions of 18×1 µm^2, 16×1.1 µm^2, and 13×1 µm^2 respectively. The devices are designed by manipulating the phase and amplitude of all possible eigenmodes supported in the waveguide, which is inherently scalable and versatile for on-chip mode and wavefront manipulation. The unique properties of metamaterials provide powerful tools for on-chip polarization manipulation and offer new possibilities for the development of compact and high-performance photonic integrated circuits.
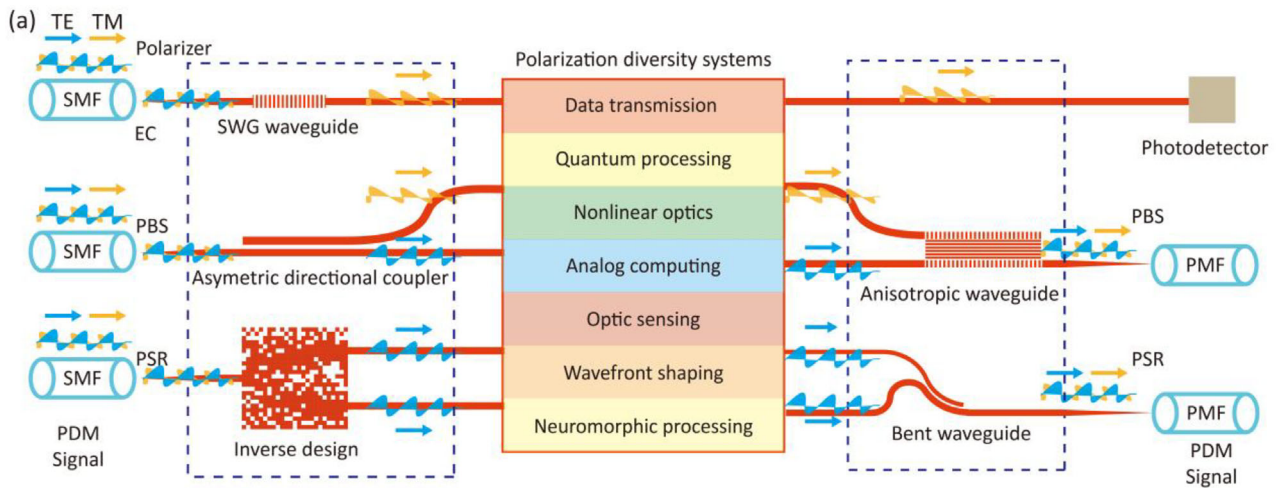
1. Introduction

Silicon photonics has been widely explored in various fields due to its complementary metal-oxide-semiconductor (CMOS) compatibility, high refractive-index contrast, and cost-effectiveness.[1,2] Additionally, its high birefringence, which leads to different behaviors between transverse electric (TE) and transverse magnetic (TM) modes, has laid a ground foundation for the development of polarization diversity systems. On-chip polarization manipulation has shown significant impacts in a range of applications, it can double transmission data streams for communication systems,[3] enable efficient scaling of the capacity for computing and processing systems,[4,5] assist in phase-matching conditions for nonlinear wavelength conversion,[6,7] enhance signal detection for optical sensing systems,[8] and allow precise

adjustment in wavefront shaping for vortex beam generation,[9] as shown in **Figure 1**a.

In recent years, numerous on-chip structures have been reported to construct high-performance polarization-handing components. For example, asymmetric directional couplers (ADCs) are commonly used for polarization manipulation by matching the effective indices of TM and TE modes in adjacent waveguides.[10–26] It provides the best overall performance, while high fabrication accuracy is usually required. Adiabatic coupling is another widely studied method for polarization conversion, achieved by polarization hybridization processes with asymmetric structure along the vertical direction. It can be applied for robust polarization rotation but may suffer from large device scale or fabrication complexity.[27]

Beyond classical waveguide-based architectures, metamaterials have gained more attention in recent years due to their unprecedented optical manipulation capabilities in subwavelength scales. For example, subwavelength grating (SWG) metamaterial offers artificial refractive indices and engineered dispersion to construct waveguides, enabling novel optical behavior. SWG is widely employed in various fields including polarization manipulation, with advantages such as board bandwidth and larger fabrication tolerance.[28–39] Recently, inverse-designed metamaterial has also been utilized to design on-chip functional components, allowing computers to optimize the structure using various numerical algorithms. This method can optimize the structures extensively with large degrees of design freedom to maximize device performance. However, the optimization processes can be time-consuming, and some freeform structures might pose fabrication challenges.[40–44] On the other hand, gradient index dielectric metamaterials have provided a forward-designed approach to manipulate waveguide mode-order conversions.[45–49] By offering desired phase distribution to satisfy the phase-matching conditions between different modes, it is possible to achieve high-efficiency mode-order conversions with clear physical guidelines. However, these designs mainly focus on the coupling between different mode orders in the same polarization, and the manipulation of different polarization has yet to be explored.

In this paper, we expand the functionalities of gradient index dielectric metamaterials to achieve full-space polarization manipulation. The dielectric metamaterials patterned on strip

Y. Zhao, J. Xiang, A. He, Y. He, X. Guo, Y. Su
State Key Laboratory of Advanced Optical Communication Systems and Networks Department of Electronic Engineering
Shanghai Jiao Tong University
Shanghai 200240, China
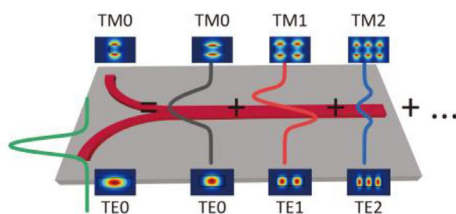E-mail: guoxuhan@sjtu.edu.cn
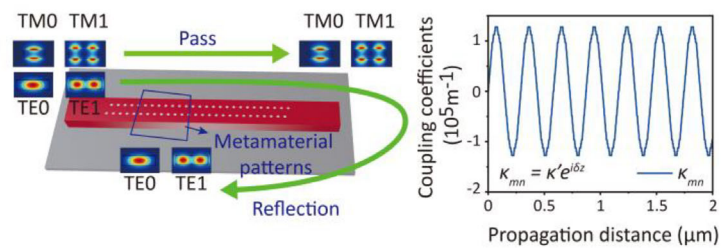
Figure 1. Integrated polarization-diversity systems and the fundamental principles. a) On-chip polarization manipulation techniques and polarization-diversity circuit scenarios. SMF single-mode fiber, PMF polarization-maintaining fiber, EC edge coupler, PDM polarization division multiplexing, SWG subwavelength grating, PBS polarizati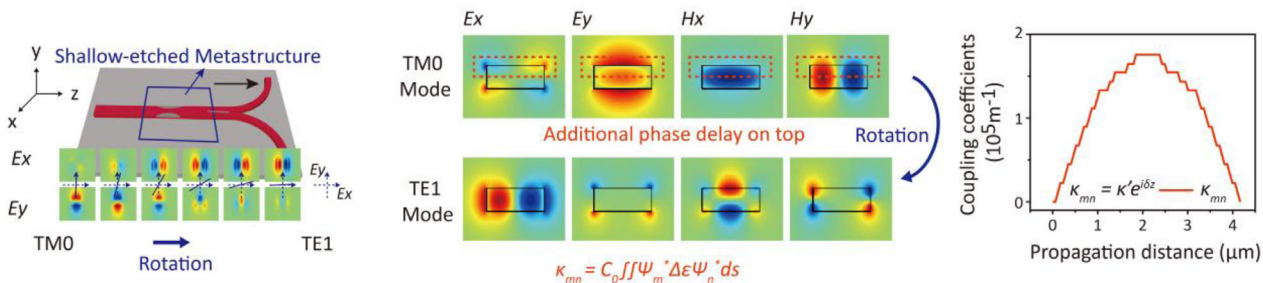on beam splitter, PSR polarization-splitter-rotator. b) The propagating field within the waveguide is depicted as a superposition of all possible eigenmodes supported by the waveguide, with specific amplitudes and phases. c) The metamaterial provides periodic coupling coefficients and enables contra-directional coupling. d) The shallow-etched meta-structure on the top surface of the waveguide induces phase delays for achieving polarization rotation. The metamaterial also induces suitable coupling coefficients for efficient polarization rotation.

waveguides can help to satisfy the phase-matching conditions, which enables the coupling between selected modes. The positions of the metamaterials are utilized to manipulate the phase of different polarized modes in the waveguide, which further influence the light spatial distribution within the waveguide. We have fully demonstrated polarization-handling devices, including polarizer, polarization beam splitter (PBS), and polarization-splitter-rotator (PSR). The proposed polarizer features a high extinction ratio (ER) of > 35 dB, with an insertion loss (IL) of < 1 dB and a compact footprint of 18×1 μm^2. The proposed PBS

also features a low crosstalk of > 30 dB, with an IL of < 2 dB and a compact footprint of 16×1.1 μm^2. The PSR features a compact footprint of 13×1 μm^2, with IL of < 1.3 dB and ER of > 12 dB.

2. Principle and Design

2.1. Basic Principle

The birefringence is widespread in photonic integrated circuits, which leads to different behaviors of TE-polarized and

**ADVANCED
SCIENCE NEWS**

www.advancedsciencenews.com

LASER
& PHOTONICS
REVIEWS

www.lpr-journal.org

TM-polarized light [see Section S1 of the Supporting Information]. Here the metamaterial is employed to manipulate the phase distribution of the propagating light [see Section S2 of the Supporting Information], further controlling the polarization state in a photonic integrated circuit. This is achieved through the principles of mode expansion, mode coupling, and polarization rotation.

The mode expansion procedures enable the calculation of the power distribution in the waveguide in terms of possible eigenmodes. As shown in Figure 1b, the propagating field in the waveguide can be decomposed into the eigenmodes, whose amplitude and phase are described in Equation 1:

$$E(x, y, z) = \sum_m \mathcal{A}_m(z) \Psi_m(x, y) e^{-i\beta_m} \tag{1}$$

where $A_m(z)$ represents the complex transmission coefficient of the mth-order mode along the propagation distance, β_m and $\Psi_m(x,y)$ represents the propagation constant and electric field distribution respectively.

The mode conversion and polarization rotation processes will change the contribution of different modes in the waveguide. According to the classical coupled-mode theory (CMT) [see details in Section S3 of the Supporting Information], the dielectric perturbation nanoholes and nanoslots are mathematically described by coupling coefficients κ as Equation 2:[51]

$$\kappa_{mn}(z) = \frac{\omega}{4} \iint \Psi_m^*(x, y) \, \Delta\varepsilon(x, y, z) \, \Psi_n(x, y) \, dx dy \tag{2}$$

where $\Delta\varepsilon(x,y,z)$ represents the dielectric perturbation as described in Equation 3:[50]

$$\Delta\varepsilon(x, y, z) = \begin{cases} \varepsilon_0 \left(n_{\mathrm{Die}}^2 - n_{\mathrm{Si}}^2 \right); & \text{if there is dielectric material;} \\ 0; & \text{otherwise} \end{cases} \tag{3}$$

The ϵ_0 is the free space permittivity, n_{Si} and n_{Die} are the refractive index of the silicon and the dielectric material of silica, respectively. Then the evolution of the transmission coefficient coefficients $A_m(z)$ can be driven by the CMT equations as the following Equation 4:[51]

$$\frac{dA_n(z)}{dz} = -i \sum_n \kappa_{mn}(z) A_n(z) e^{-i(\beta_n - \beta_m)z} \tag{4}$$

Hence, as the transmission coefficient of each mode $A_m(z)$ is calculated, the metamaterial can manipulate the coupling between different polarized modes, and the power of each mode can be obtained in terms of the coupling coefficients as $|A_m(z)|^2$.

The contra-directional coupling process, as shown in Figure 1c, involves the coupling of two modes in opposite propagation directions. This coupling process is governed by periodic coupling coefficients derived from periodic perturbations as Equations 2 and 3. The coupling coefficients with the period of Λ can compensate for the phase mismatch as $2\pi / \Lambda = \beta_n + \beta_m$, resulting in the selected polarized mode being reflected.

The polarization rotation, as illustrated in Figure 1d, is achieved by the shallow-etched meta-structures on the top surface of the waveguide. The polygons induce additional phase delays in the propagating light, leading to a reshaped phase distri-

bution and mode rotation from TM_0 to TE_1. This process can be described by the CMT. Due to the limited waveguide width, the TE or TM modes have a small existence of E_x component for TM mode or E_y component for TE mode. These components enable the generation of non-zero coupling coefficients assisted with the shallow-etched perturbations as Equation 2, leading to polarization coupling between the TE_1 and TM_0 modes as Equation 4.

By combining these principles with the unique optical properties of metamaterials, it is possible to achieve precise and efficient control over the polarization state of light in a compact on-chip device. In this paper, the proposed polarization-handling components including polarizer, PBS, and PSR are designed based on a regular silicon-on-insulator (SOI) platform, which consists of a 220-nm thick top silicon layer, a 3-µm thick buried silica layer, and a 1-µm thick cladding silica layer. The designs are explained in detail as follows [see also in Section S4 of the Supporting Information].

2.2. Polarizer

The proposed polarizer is designed to selectively block the forward-propagating TE_0 mode while allowing the TM_0 mode to pass through. The proposed polarizer consists of a multimode

waveguide patterned by two arrays of periodic fully-etched dielectric holes as shown in **Figure 2**ai,bi. The utilization of metamaterial structures enables the coupling of the TE_0 mode into the backward-propagating TE_1 mode, without affecting the input TM_0 mode.

The top and bottom arcs of each hole are defined as half of a sinusoidal function, and the waveguide width w_1 is set to 1 µm to accommodate both the TE_0 and TE_1 modes. The vertical diameter of hole a_1 is set to 500 nm for large coupling coefficients, which leads to large bandwidth and high ER. Note that larger diameters may also lead to increased ILs. The coupling length of 16 µm is chosen to balance the trade-off between the coupling length and the ER. The period Λ of the hole arrays is 390 nm to satisfy the phase-matching condition between the TE_0 and TE_1 mode, as determined by the equation $\Lambda = \lambda / (n_0 + n_1)$, where n_0 and n_1 is the effective index of TE_0 and TE_1 mode respectively. **Table 1** provides a summary of the detailed parameters.

The three-dimensional finite-difference time-domain (3D-FDTD) method is implemented to verify the theoretical results of the device. Figure 2ci shows the normalized power distributions of the TM_0 and TE_0 modes respectively. The input TM_0 mode goes through the waveguide as expected, while the input TE_0 mode is effectively blocked. This is further evidenced by the fast vanishing of the input TE_0 mode in the metamaterial-patterned waveguide, as shown in the zoomed-in panel. The spectra of different polarized modes are displayed in Figure 2di, which indicates that the device has a low IL of 0.64 dB and a high ER of 38 dB at 1550 nm. The device also exhibits low IL below 1.2 dB and high ER >30 dB over the wavelength range from 1410 nm to 1690 nm.

2.3. Polarization Beam Splitter (PBS)

The proposed PBS is utilized to separate the input TE_0 mode and TM_0 mode into different output ports. Figure 2aii illustrates the
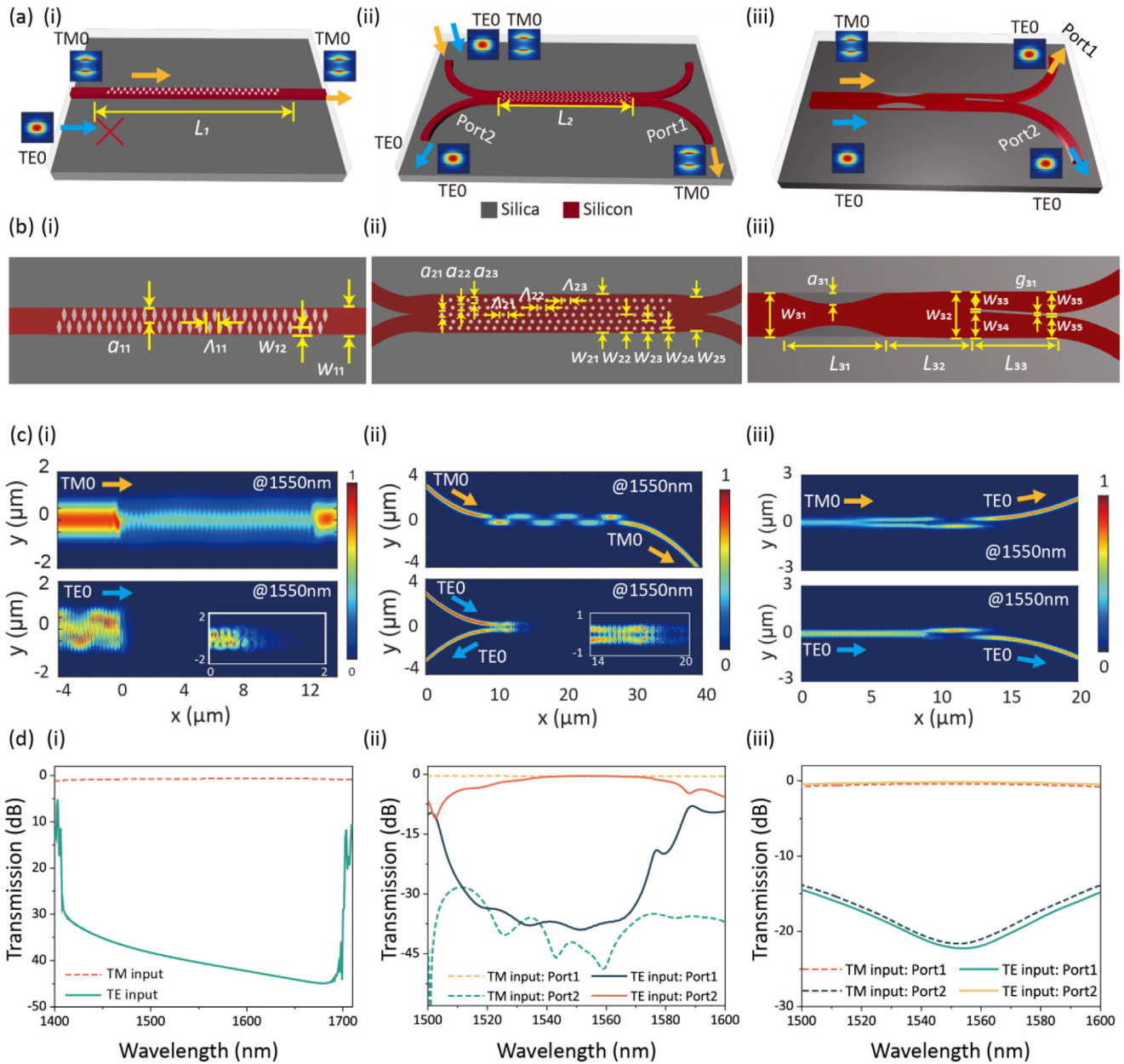
Figure 2. The schematic and simulated results of the proposed polarizer, PBS and PSR. a) The schematic, b) top view c) simulated power distribution of the central cross-section at 1550 nm, and d) simulated spectral responses of the proposed i) polarizer, ii) PBS, and iii) PSR. The polarizer blocks the input TE_0 mode and passes the TM_0 mode. The PBS directs the input TM_0 mode to port 1 and the input TE_0 mode to port 2. The PSR rotates the input TM_0 mode to the TE_0 mode at port 1 and directs the input TE_0 mode to port 2.

Table 1. Parameters of the Proposed Metamaterial-assisted Polarization-handling Devices.

Legend: Parameter [unit]							
Polarizer	a_{11}: 500 nm	Λ_{11}: 390 nm	w_{11}: 1 μm	w_{12}: 250 nm	L_1: 18 μm		
PBS	a_{21}: 100 nm	a_{22}: 80 nm	a_{23}: 120 nm	w_{21}: 1.1 μm	w_{22}: 550 nm	w_{23}: 360 nm	w_{24}: 200 nm	w_{25}: 1 μm
	Λ_{21}: 328 nm	Λ_{22}: 370 nm	Λ_{23}: 446 nm	L_2: 16 μm			
PSR	a_{31}: 150 nm	L_{31}: 7.06 μm	L_{32}: 1.4 μm	L_{33}: 4.36 μm	w_{31}: 700 nm	w_{32}: 800 nm	w_{33}: 300 nm	w_{34}: 400 nm
	w_{35}: 350 nm	g_{31}: 100 nm					

**ADVANCED
SCIENCE NEWS**

www.advancedsciencenews.com
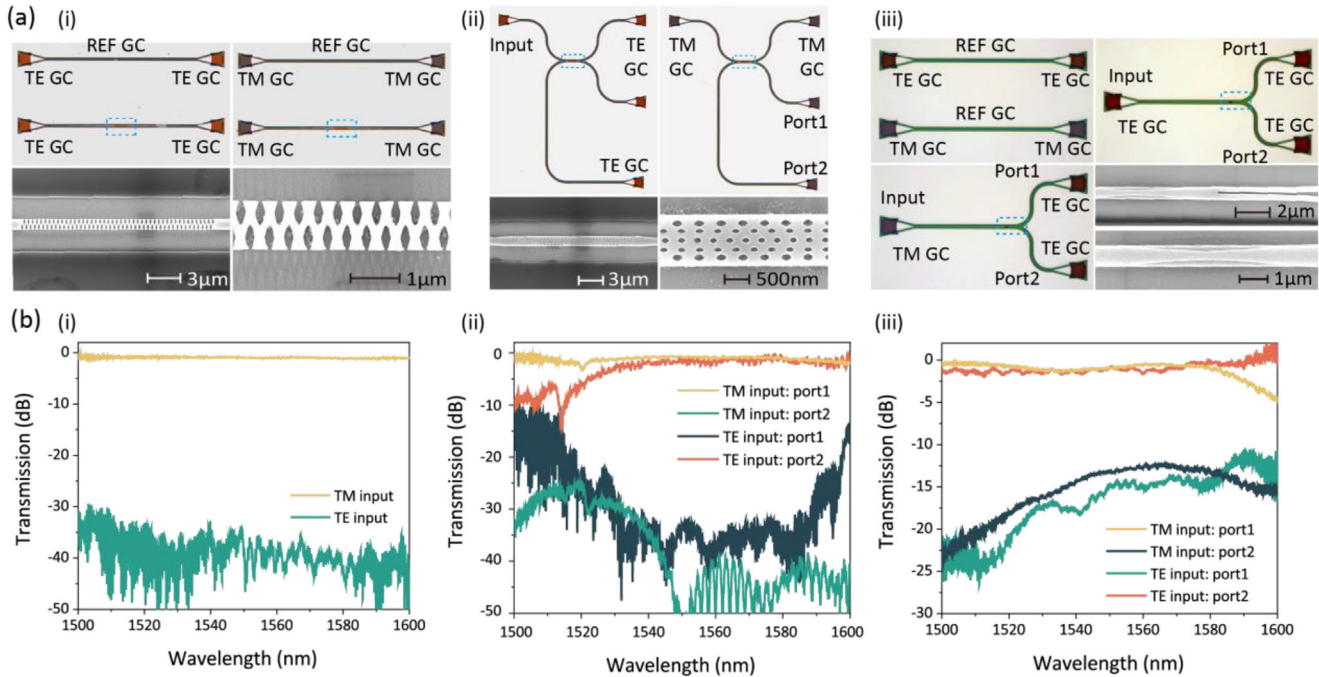
LASER
& PHOTONICS
REVIEWS

www.lpr-journal.org

Figure 3. Fabricated structures and measured results. a) The optical microscope and scanning electron microscope (SEM) images of the fabricated metamaterial-based i) polarizer, ii) PBS, and iii) PSR. Different kinds of grating couplers are employed for the coupling of different polarized modes. b) Measured transmission at different ports for the fabricated i) polarizer, ii) PBS, and iii) PSR.

schematic of the proposed PBS, which is composed of four bending waveguides connected with a bus waveguide. The bus waveguide is patterned by metamaterials composed of five periodically fully-etched hole arrays. The metamaterials allow for the manipulation of power coupling between forward and backward propagation modes as well as their phase delay, which further influences the electromagnetic profiles in the waveguide. The detailed steps are explained as follows:

i. When the TE_0 mode from the single-mode bend waveguide couples into the multimode bus waveguide, the input field can be described as a superposition of all possible eigenmodes as Equation 1. Here only TE_0, TE_1, and TE_2 modes are excited and limited by the waveguide width. The TM modes are not excited due to their negligible mode overlap.

ii. As the TE_0, TE_1, and TE_2 modes propagate in the bus waveguide, they are reflected into backward-propagating TE_0, TE_1, and TE_2 modes respectively by three groups of nanohole arrays with period $\Lambda_1 = \lambda / 2n_0$, $\Lambda_2 = \lambda / 2n_1$ and $\Lambda_3 = \lambda / 2n_2$, where n_i represents the effective index of the ith-order mode. The three groups of nanoholes can help to satisfy the phase-matching conditions between the forward and backward TE_0, TE_1, and TE_2 modes simultaneously.

iii. The phase differences between the reflected modes are controlled by the relative position of the hole arrays. The relative position of the nanohole arrays for TE_1 mode is set 220 nm behind, which introduces an extra π phase delay of the reflected TE_1 mode. This phase delay causes the reflected light to focus on the other port due to the symmetry property of the structure and mode profiles.

For the input TM_0 mode, the metamaterial patterned structure acts as a homogeneous material, and the input light is first expended into TM_0 and TM_1 mode in the multimode waveguide. The phase differences are controlled by the coupling length resulting from mode dispersion. After several half-beat lengths, the light is ultimately guided into the through port. Table 1 provides a summary of the design parameters.

Figure 2cii shows the simulated power distribution of the proposed device at 1550 nm. The launched TM_0 mode directly passes through the metamaterial waveguide and couples into port 1, while the launched TE_0 mode is reflected and coupled into port 2. The zoomed-in panel also shows that the input TE_0 mode quickly vanishes in the metamaterial waveguide. Figure 2dii shows the simulated spectra. For the TE_0 mode, the device has a low IL of < 1 dB and a high ER >30 dB from 1530 nm to 1570 nm, with a loss of 0.39 dB and ER of 38.8 dB at 1550 nm. For the TM_0 mode, the IL is < 0.6 dB and ER >28 dB from 1500 nm to 1600 nm, with a loss of 0.47 dB and ER of 42.5 dB at 1550 nm.

2.4. Polarization-Splitter-Rotator (PSR)

The proposed PSR divides the input TE_0 mode and TM_0 mode and rotates the polarization state of the TM_0 mode. The PSR is composed of two bending waveguides that are connected to a bus waveguide, which is patterned by a fully-etched slot and 70 nm shallow-etched meta-structures. Figure 2aiii provides a schematic illustration of the proposed PSR. The shallow-etched polygons have the same depth as the grating couplers (GCs), which helps to simplify the fabrication process.

In the first section of the proposed device, the meta-structures induce a phase delay for the light on the top for the TM_0 mode, which leads to the mode rotation. The meta-structures cause an overlap between the TM_0 and TE_1 modes in the waveguide and induce a coupling coefficient that compensates for the phase mismatch calculated by Equation 2. This leads to a gradual conversion from TM_0 mode to TE_1 mode as described by Equation 4. In contrast, the TE_0 mode remains unchanged due to the symmetrical mode profile and structure. The coupling coefficient is always zero according to Equation 2, indicating no mode coupling occurs and the TE_0 mode is not affected by the meta-structures.

In the second section, the TE_0 and TE_1 modes are demultiplexed into different ports through a fully-etched slot. The bus waveguide is divided into two waveguides with different widths by the slot, which results in different phase delays for the light in the upper and bottom waveguides. The light with different phase delays is reshaped into different ports.[45] The dielectric slot also helps to satisfy the phase-matching condition, more detailed information can be obtained in our previous work.[45] The detailed parameters of the proposed PSR are summarized in Table 1.

Figure 2ciii shows the simulated power distribution of the proposed device at 1550 nm. The TM_0 mode first converts into the TE_1 mode and couples into the upper port, while the TE_0 mode remains unchanged and couples into the bottom waveguide. Figure 2diii displays the simulated spectra response of the structure. The results indicate that the device has a low IL of < 0.8 dB and high ER >10 dB for the TE_0 mode from 1500 nm to 1600 nm, with a loss of 0.37 dB and ER of 18 dB at 1550 nm. Similarly, for the TM_0 mode, the ILs are < 0.7 dB with ER >10 dB from 1500 nm to 1600 nm, with a loss of 0.43 dB and ER of 16 dB at 1550 nm. The TE-polarized light in the two output ports exhibits a mode purity of over 98% in simulation.

3. Fabrication and Characterization

The proposed metamaterial-based polarization-handling devices are fabricated on an SOI platform. Microscope images of the fabricated polarizers, PBS, and PSR are presented in **Figure 3**a. These devices are characterized by an optical power meter (Santec MPM210) and a tunable laser (Santec TSL770). GCs are utilized to couple light between fibers and silicon waveguides, which determine the light polarization in the waveguide by their period and duty cycle. Two sets of devices with the same parameters are fabricated closely with either TE or TM-type GCs, and reference TE- and TM-type GCs are also fabricated closely on the same chip. Detailed information on the device fabrication, characterization, and data normalization can be found in Sections S5–S7 of the Supporting Information respectively.

As shown in Figure 3(ai,bi), the polarizer blocks the TE-polarized light and unblocks the TM-polarized light. The ILs are <1 dB and the ER is >30 dB in the range of 1500 to 1600 nm, with a loss of 0.8 dB and ER of 40 dB at 1550 nm. The PBS in Figure 3aii reflects the TE-polarized light and guides it into port 1, and couples the TM-polarized light into port 2. The TE-polarized mode has ILs of <2 dB and ER >30 dB in the range of 1540 to 1590 nm, with a loss of 1.5 dB and ER of 32 dB at 1550 nm. The TM-polarized mode has ILs of <1.4 dB and ER >33 dB in the range of 1540 to 1590 nm, with a loss of 0.8 dB and ER of 45 dB at 1550 nm. The PSR in Figure 3aiii rotates the TM-polarized mode

Table 2. Performance Comparison of Silicon Polarization-handling Components.

Function	Structure	Coupling region [µm²]	IL [a] [dB]	ER [b] [dB]	BW [c] [nm]	Exp. or Sim.
Polarizer:	ADC [d] [10]	6.6 × 1.8	< 0.7	> 15	80	Exp.
	Adiabatically bend [27]	63 × 9.5	< 0.4	> 27	100	Exp.
	Anisotropic SWG bend [28]	13 × 6.5	< 1	> 20	415	Exp.
	SWG waveguide[30]	9 × 0.6	< 1	> 20	60	Exp.
	SWG waveguide[31]	60 × 1.1	< 0.4	> 30	100	Exp.
	Bragg gratings [32]	30 × 1	< 0.13	> 30	61	Sim.
	Periodically structured waveguides [33]	21 × 0.5	< 1	> 30	90	Exp.
	1D photonic crystals [39]	4 × 0.7	< 1	> 20	50	Exp.
	This work	18 × 1	< 1	> 35	100	Exp.
PBS:	Bridged ADC [12]	29.4 × 2	< 1	> 25	60	Exp.
	SWG ADC [13]	4 × 2.5	< 2.8	> 15	60	Exp.
	GACDC [f] [14]	27.5 × 1.1	< 1	> 30	21	Exp.
	Bend DC [15]	20 × 6.9	< 0.5	> 30	70	Exp.
	SWG ADC [18]	6.45 × 1.5	< 1	> 20	100	Sim.
	Bent ADC [20]	8.7 × 3	< 1	> 18	41	Exp.
	Adiabatic ADC [25]	11 × 1.2	< 1	> 25	120	Exp.
	SWG bridged ADC [34]	33.6 × 1.9	< 1	> 20	220	Exp.
	Anisotropic SWG DC [35]	12.3 × 1.9	< 1	> 25	175	Exp.
	SWG MMI [29]	14.6 × 1.5	< 1	> 15	40	Sim.
	Inverse design ADC[40]	48 × 2.3	< 0.58	> 15	250	Sim.
	Inverse design [43]	2.4 × 2.4	< 1.6	> 10	32	Exp.
	MMI [e] [52]	600 × 7	< 3	> 20	20	Exp.
	This work	16 × 1.1	< 2	> 30	50	Exp.
PSR:	Adiabatic with ADC [19]	70 × 1.3	<1.5	>15	80	Exp.
	Bent ridged ADC [21]	10.74 × 5	< 0.4	> 18	100	Exp.
	Taper + Bent ADC [22]	47.5 × 1.5	< 1	> 20	85	Exp.
	Taper + counter ADC [23]	313.5 × 1.5	< 1.21	> 12.1	110	Exp.
	Taper ADC [24]	375 × 1.5	< 1	> 10	85	Exp.
	Taper + ADC [26]	475 × 1.4	< 1.6	> 13	50	Exp.
	Double-etched ADC [11]	27 × 1.4	< 0.5	> 20	30	Exp.
	SWG taper ADC [36]	171 × 1.6	< 1.4	> 15	70	Exp.
	SWG ADC [37]	25 × 1.2	< 1	> 10	90	Sim.
	SWG taper ADC [38]	5.5 × 1.35	< 0.63	> 14.3	95	Sim.
	Inverse design [44]	7.92 × 2.4	< 0.2	> 20	40	Exp.
	This work	13 × 1	< 1.3	> 12	80	Exp.

[a] IL: Insertion loss; [b] ER: Extinction ratio; [c] BW: Bandwidth; [d] ADC: asymmetric directional coupler; [e] MMI: Multimode interference coupler; [f] GACDC: Grating-assisted contra-directional coupler.

and coupled it to port 1, and couples the TE-polarized mode into port 2. The device has ILs of < 1.3 dB and ER > 12 dB in the range of 1500 to 1580 nm, with a loss of <1 dB and ER >13 dB at 1550 nm for both the TE- and TM-polarized modes. The measured losses of the devices are slightly larger than the simulated results, possibly due to unexpected scattering losses from waveguide sidewall roughness and fabrication errors. The measured results largely conformed to the simulated result, except for a blue wavelength shift in the PSR. This discrepancy can be attributed to the narrower fabricated waveguide width, and the PSR is more
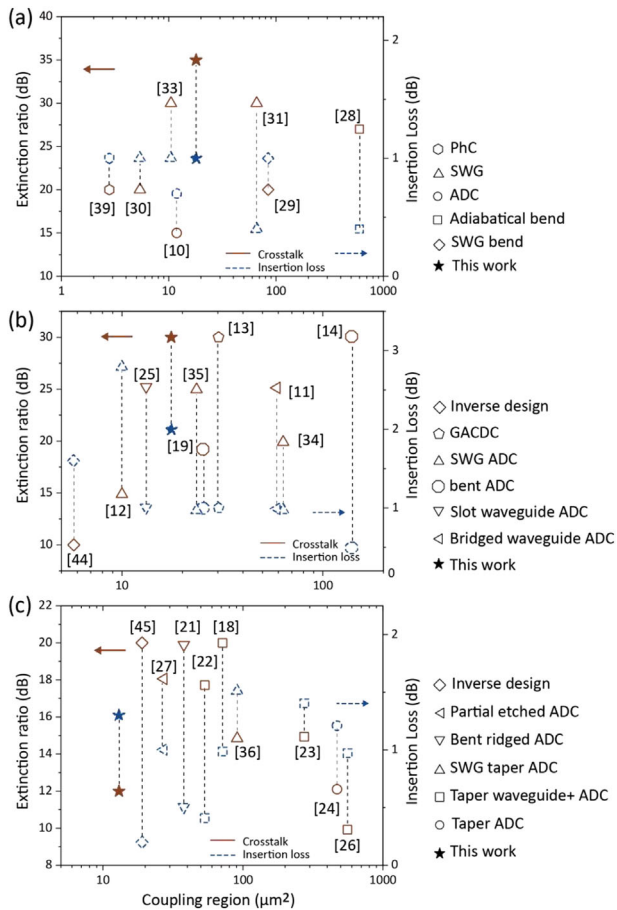
**ADVANCED
SCIENCE NEWS**

www.advancedsciencenews.com

LASER
& PHOTONICS
REVIEWS

www.lpr-journal.org

Figure 4. Comparison of state-of-the-art on-chip polarization-handling devices. The comparison is focusing on the extinction ratio and insertion loss versus coupling region. The analyzed devices include a) polarizers, b) PBS, and c) PSR. The results demonstrate that the proposed metamaterial-assisted polarization-handling devices offer competitive performance while maintaining compact device footprints. PhC: photonic crystal; ADC: asymmetric directional coupler; GACDC: grating-assisted contra-directional coupler.

sensitive to fabrication errors. The fabrication tolerant analysis is provided in Section S8 of the Supporting Information.

Table 2 compares the performance of previously reported state-of-the-art polarization-handling components. The results indicate that the proposed metamaterial-assisted polarization-handling devices exhibit competitive performance with full space manipulation while maintaining a compact device footprint. **Figure 4** also provides a visual representation to compare the experimentally demonstrated works. Another comparison focusing on the polarization rotation process can be found in Section S9 of the Supporting Information.

4. Conclusion

In this paper, the metamaterial-assisted polarization-handling devices have demonstrated full control over the polarization state of light with competitive performance and ultra-compact footprints, which offer a significant advancement in the field of optical manipulation. These novel metamaterials can provide de-

signed coupling coefficients between different polarized modes and alter the phase delay at various positions, hence enabling compensation for their phase mismatch and effective control over the power distribution of the light, respectively. As such, fully polarization-manipulating devices, including the polarizer, PBS, and PSR, with compact waveguide lengths of 18, 16, and 13 μm respectively, are demonstrated with low IL and high ER. These metamaterial-assisted design methods may also help to build a comprehensive physical model to choose the design region and initial pattern for the inverse design method, and the performance can be further improved with optimization. These metamaterial-assisted design methods may hold great potential for the development of various applications in photonics, including polarization diversity circuits, nonlinear photonics, optical analog computing, and beyond.

Supporting Information

Supporting Information is available from the Wiley Online Library or from the author.

Conflict of Interest

The authors declare no conflict of interest.

Data Availability Statement

The data that support the findings of this study are available from the corresponding author upon reasonable request.

[1] P. Dong, Y. K. Chen, G. H. Duan, D. T. Neilson, *Nanophotonics* **2014**, *3*, 215.
[2] S. Y. Siew, B. Li, F. Gao, H. Y. Zheng, W. Zhang, P. Guo, S. W. Xie, A. Song, B. Dong, L. W. Luo, C. Li, X. Luo, G. Q. Lo, *J. Light. Technol.* **2021**, *39*, 4374.
[3] P. Dong, C. Xie, L. Chen, L. L. Buhl, Y.-K. Chen, *Opt. Express* **2012**, *20*, B624.
[4] L.-T. Feng, M. Zhang, Z.-Y. Zhou, M. Li, X. Xiong, L. Yu, B.-S. Shi, G.-P. Guo, D.-X. Dai, X.-F. Ren, others, *Nat. Commun.* **2016**, *7*, 11985.

[5] D. V. Sychev, A. E. Ulanov, E. S. Tiunov, A. A. Pushkina, A. Kuzhamuratov, V. Novikov, A. I. Lvovsky, *Nat. Commun.* **2018**, *9*, 3672.

[6] R. M. Osgood, N. C. Panoiu, J. I. Dadap, X. Liu, X. Chen, I. W. Hsieh, E. Dulkeith, W. M. J. Green, Y. A. Vlasov, *Adv. Opt. Photonics* **2009**, *1*, 162.

[7] J. Leuthold, C. Koos, W. Freude, *Nat. Photonics* **2010**, *4*, 535.

[8] D. Dai, J. Bauters, J. E. Bowers, *Light Sci. Appl.* **2012**, *1*, 1.

[9] B. Fang, Z. Wang, S. Gao, S. Zhu, T. Li, *Nanophotonics* **2021**, *11*, 1923.

[10] H. Xu, Y. Shi, *IEEE Photonics Technol. Lett.* **2017**, *29*, 861.

[11] H. Guan, A. Novack, M. Streshinsky, R. Shi, Q. Fang, A. E.-J. Lim, G.-Q. Lo, T. Baehr-Jones, M. Hochberg, *Opt. Express* **2014**, *22*, 2489.

[12] Y. Kim, M. H. Lee, Y. Kim, K. H. Kim, *Opt. Lett.* **2018**, *43*, 3241.

[13] C. Li, D. Dai, *Opt. Lett.* **2017**, *42*, 4243.

[14] Y. Zhang, Y. He, J. Wu, X. Jiang, R. Liu, C. Qiu, X. Jiang, J. Yang, C. Tremblay, Y. Su, *Opt. Express* **2016**, *24*, 6586.

[15] H. Wu, Y. Tan, D. Dai, *Opt. Express* **2017**, *25*, 6069.

[16] X. Wang, X. Quan, W. Zhang, J. Hu, C. Shen, X. Cheng, *IEEE Photonics J* **2018**, *10*, 1.

[17] C. Li, M. Zhang, J. E. Bowers, D. Dai, *Opt. Lett.* **2020**, *45*, 2259.

[18] S. Dai, J. Xiao, *Appl. Opt.* **2022**, *61*, 126.

[19] D. Dai, H. Wu, *Opt. Lett.* **2016**, *41*, 2346.

[20] Y. Zhang, Y. He, X. Jiang, B. Liu, C. Qiu, Y. Su, R. A. Soref, *APL Photonics* **2016**, *1*, 091304.

[21] K. Tan, Y. Huang, G.-Q. Lo, C. Yu, C. Lee, *Opt. Express* **2017**, *25*, 3234.

[22] H. Xu, Y. Shi, *Opt. Express* **2017**, *25*, 18485.

[23] Y. Zhao, C. Qiu, A. Wu, H. Huang, J. Li, Z. Sheng, W. Li, X. Wang, F. Gan, *IEEE Photonics J.* **2019**, *11*, 1.

[24] A. Melikyan, P. Dong, *APL Photonics* **2019**, *4*, 030803.

[25] Y. Tian, J. Qiu, C. Liu, S. Tian, Z. Huang, J. Wu, *Opt. Express* **2019**, *27*, 999.

[26] W. D. Sacher, T. Barwicz, B. J. F. Taylor, J. K. S. Poon, *Opt. Express* **2014**, *22*, 3777.

[27] H. Zafar, P. Moreira, A. M. Taha, B. Paredes, M. S. Dahlem, A. Khilo, *Opt. Express* **2018**, *26*, 31850.

[28] H. Xu, D. Dai, Y. Shi, *Photonics Res.* **2019**, *7*, 1432.

[29] L. Liu, Q. Deng, Z. Zhou, *Opt. Lett.* **2016**, *41*, 5126.

[30] X. Guan, P. Chen, S. Chen, P. Xu, Y. Shi, D. Dai, *Opt. Lett.* **2014**, *39*, 4514.

[31] Y. Xiong, D.-X. Xu, J. H. Schmid, P. Cheben, N. Y. Winnie, *IEEE Photonics J.* **2015**, *7*, 1.

[32] S. Wu, J. Hao, Z. Zhao, X. S. Yao, *Opt. Express* **2021**, *29*, 27640.

[33] H. Zafar, M. Odeh, A. Khilo, M. S. Dahlem, *IEEE Photonics Technol. Lett.* **2020**, *32*, 1029.

[34] H. Xu, D. Dai, Y. Shi, *Laser Photonics Rev.* **2019**, *13*, 1800349.

[35] Y. Xu, J. Xiao, *Opt. Lett.* **2016**, *41*, 773.

[36] S. Homan, F. A. N. Z. Hang, N. I. A. F. J. Aeger, L. Ukas, C. Hrostowski, *Opt. Express* **2019**, *27*, 17581.

[37] Y. Xiong, J. G. Wangüemert-Pérez, D.-X. Xu, J. H. Schmid, P. Cheben, W. N. Ye, *Opt. Lett.* **2014**, *39*, 6931.

[38] J. Chen, J. Xiao, *J. Opt. Soc. Am. B* **2022**, *39*, 345.

[39] D. W. Kim, M. H. Lee, Y. Kim, K. H. Kim, *Opt. Express* **2016**, *24*, 21560.

[40] P. H. Fu, T. Y. Huang, K. W. Fan, D. W. Huang, *IEEE Photonics J* **2019**, *11*, 1.

[41] W. Chang, S. Xu, M. Cheng, D. Liu, M. Zhang, *Opt. Express* **2020**, *28*, 28343.

[42] Z. Yu, H. Cui, X. Sun, *Opt. Lett.* **2017**, *42*, 3093.

[43] B. Shen, P. Wang, R. Polson, R. Menon, *Nat. Photonics* **2015**, *9*, 378.

[44] Y. Liu, S. Wang, Y. Wang, W. Liu, H. Xie, Y. Yao, Q. Song, X. Zhang, Y. Yu, K. Xu, *Opt. Lett.* **2019**, *44*, 4495.

[45] Y. Meng, Y. Chen, L. Lu, Y. Ding, A. Cusano, J. A. Fan, Q. Hu, K. Wang, Z. Xie, Z. Liu, Y. Yang, Q. Liu, M. Gong, Q. Xiao, S. Sun, M. Zhang, X. Yuan, X. Ni, *Light Sci. Appl.* **2021**, *10*, 235.

[46] Z. Li, M. Kim, C. Wang, Z. Han, S. Shrestha, A. C. Overvig, M. Lu, A. Stein, A. M. Agarwal, M. Lon, N. Yu, *Nat. Nanotechnol.* **2017**, *12*, 675.

[47] Y. Zhao, J. Xiang, Y. He, X. Guo, Y. Su, *Eur. Conf. Opt. Commun. ECOC* **2020**, 1.

[48] Y. Zhao, X. Guo, Y. Zhang, J. Xiang, K. Wang, H. Wang, Y. Su, *Opt. Lett.* **2020**, *45*, 3797.

[49] Y. Zhao, J. Xiang, Y. He, Y. Yin, A. He, Y. Zhang, Z. Yang, X. Guo, Y. Su, *Laser Photonics Rev.* **2022**, *16*, 2200005.

[50] B. E. Abu-Elmaaty, M. S. Sayed, R. K. Pokharel, H. M. H. Shalaby, *Appl. Opt.* **2019**, *58*, 1763.

[51] G. Lifante, *Integrated Photonics: Fundamentals*, John Wiley & Sons, Hoboken, NJ, USA **2003**.

[52] Y. Huang, Z. Tu, H. Yi, Y. Li, X. Wang, W. Hu, *Opt. Eng.* **2013**, *52*, 077103.